nature photonics

ARTICLES

https://doi.org/10.1038/s41566-019-0373-y

# Self-stabilizing photonic levitation and propulsion of nanostructured macroscopic objects

Ognjen Ilic and Harry A. Atwater*

**Light is a powerful tool to manipulate matter, but existing approaches often necessitate focused, high-intensity light that limits the manipulated object's shape, material and size. Here, we report that self-stabilizing optical manipulation of macroscopic—millimetre-, centimetre- and even metre-scale—objects could be achieved by controlling the anisotropy of light scattering along the object's surface. In a scalable design that features silicon resonators on silica substrate, we identify nanophotonic structures that can self-stabilize when rotated and/or translated relative to the optical axis. Nanoscale control of scattering across a large area creates restoring behaviour by engineering the scattered phase, without needing to focus incident light or excessively constrain the shape, size or material composition of the object. Our findings may lead to platforms for manipulating macroscopic objects, with applications ranging from contactless wafer-scale fabrication and assembly, to trajectory control for ultra-light spacecraft and even laser-propelled light sails for space exploration.**

The ability of light to exert forces and torques is the cornerstone of optical manipulation of matter. For this manipulation to be stabilizing—that is, robust to perturbations of the object's position or orientation in the light field—it must exhibit a strong enough trapping potential. Among the conventional approaches for light-based mechanical manipulation, most notably particle optical tweezing and transport[1–7], the trapping potential is realized by focusing and shaping the light beam to realize field intensity gradients that trap the particle. Such optical manipulation methods have become important research tools, with wide-ranging applications in biology and biomedicine[8,9], microfluidics[10,11] and colloidal science[12]. More recently, there has been a growing interest in levitation dynamics in optomechanical systems, including passive and active feedback schemes, for realizing quantum mechanical superposition, ground-state cooling and coherent manipulation of mechanical systems[13–19].

We highlight the limitations of some of the existing methods for mechanical manipulation of matter in Fig. 1. For example, in a conventional optical tweezer trap used for controlling nanoscale and microscale objects, stability is conferred by the optical gradient force present in a highly focused beam of laser light. However, the need for high-intensity and highly focused beams limits the size, shape and material composition of the object that is to be manipulated[3]. This also constrains the distance at which manipulation is possible ($h$) relative to the focusing aperture size ($L$). For optical tweezers, as well as other means of optical trapping that rely on shaping the beam of light to create gradient forces, these limitations stem from the need to structure the incident electromagnetic field for a particle of the appropriate material, shape and size[6]. Consequently, a key feature of laser light—the ability to remain collimated and coherent over long distances—has remained a mostly untapped opportunity for optical manipulation and propulsion.

In contrast, an unfocused beam of light can provide enough intensity to balance (or overcome) the weight associated with the mass of a macroscopic reflecting structure. Indeed, the structure does not have to be nanoscopic, microscopic or in close proximity to the aperture (Fig. 1b). However, this type of dynamics is inherently unstable. The instability of such a structure is readily apparent when a slight displacement with respect to the beam axis is considered. Such a displacement, whether by rotation or translation, results in a combination of a non-zero lateral force and a torque, which ultimately directs the object out of the beam path.

Here, we show that mechanical stability of macroscopic structures could be realized by tailoring the scattering anisotropy on the nanoscale. By incorporating nanophotonic elements with tailored anisotropic scattering that control the phase of light refracted from different points on the object's surface, we can realize self-restoring mechanical behaviour that is robust to perturbations (Fig. 1c). Thus, the macroscale geometry and shape of the object is separable from its optical functionality, the latter dictated by the photonic response on the nanoscale.

We identify the elementary building-block photonic structures required to realize a macroscopic object with self-restoring dynamics in a collimated optical beam. A key property that we seek is asymmetry in the optical response, which ensures that a restoring torque can be generated for a structure that is displaced from its equilibrium position or orientation. There are several ways such a response can be realized (Fig. 1c, inset), including through (1) superposition of scattering from arrays of nanoscale anisotropic scatterers such as Mie resonators[20,21], (2) phase-gradient metasurfaces, where the superposition of scattering phase and amplitude from each resonator element of an optical metasurface enables scattered wavefront control, (3) periodic Bloch-wave-type scatterers such as photonic crystals[22–32] or (4) larger structures described by ray optics[33]. In this work, we focus on generating the desired optical response as a collective effect and develop a class of nanophotonic elements that can exhibit passive, self-restoring dynamics (Fig. 2a).

The ability to use subwavelength nanophotonic structures to control the refraction of light across a large area creates a distinctive paradigm for optical manipulation. In this manner, many of the previously discussed constraints on the shape/focus of the incident light or the size/shape/material of the object can be alleviated. Furthermore, this approach can enable functionalities beyond what is possible with conventional optical manipulation techniques. For example, using high-power laser beams, the radiation pressure on the macroscopic structure can be much greater than its weight,

Department of Applied Physics and Materials Science, California Institute of Technology, Pasadena, CA, USA. *e-mail: haa@caltech.edu

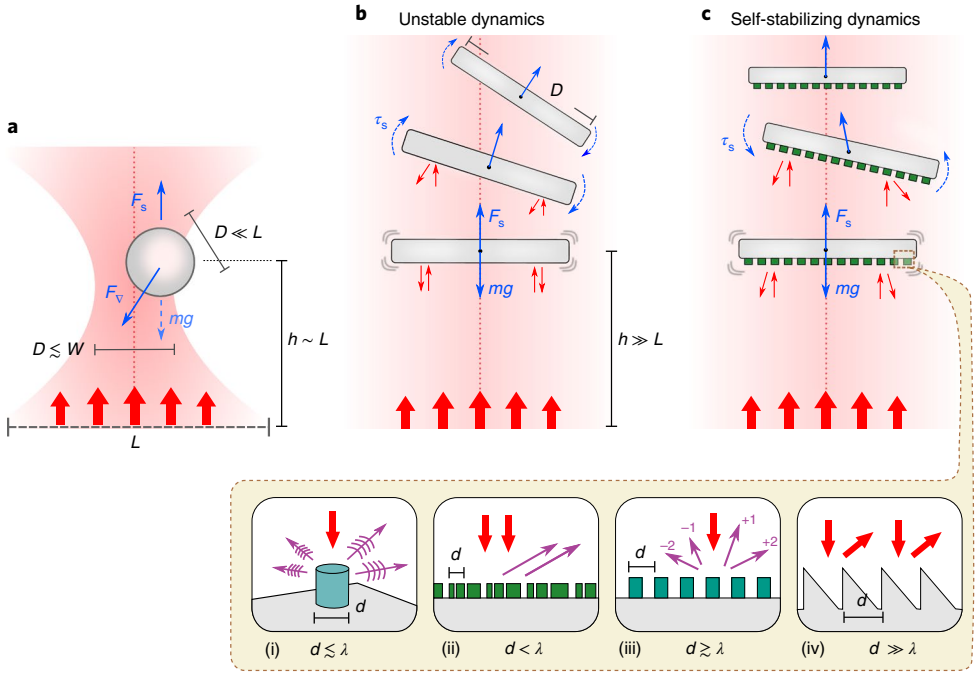


**Fig. 1 | Engineering optical anisotropy for self-stabilizing manipulation. a**,**b**, Comparing the dynamics of optical manipulation: conventional approaches such as optical tweezers (**a**) use highly focused light beams to generate the gradient force ($F_\nabla$) that overcomes the radiation pressure/scattering force ($F_s$). This limits the size of the object that can be manipulated ($D \ll L$), as well as its position ($h \sim L$), relative to the aperture size ($L$). In contrast, a collimated beam (**b**) can have enough intensity to balance a macroscopic object ($D \approx L$) at long distance (for example, $h \gg L$), but this type of dynamics is inherently unstable, with small perturbations introducing destabilizing force/torque. **c**, Engineering optical anisotropy along the surface of the object could enable self-stabilizing mechanical behaviour. This is accomplished with nanoscale metamaterial elements that facilitate asymmetric scattering of light, including individual scatterers (for example, Mie resonators) (i), phase-gradient metasurfaces (ii) and photonic crystals (iii); larger elements described by ray optics are also an option (iv). This approach could enable long-distance manipulation, levitation and even propulsion of macroscopic objects. Here, large (small) red arrows correspond to incident (scattered) light, blue arrows indicate forces/torques on the structure and purple arrows (inset) correspond to light that is scattered anisotropically.

leading to levitation or even substantial acceleration. One potential domain of application is space flight, including trajectory control for next-generation lightweight satellites or propulsion of cosmic light sails, where this approach can give rise to passive stability of the light-sail structure riding an optical beam[34–36]. Since this type of propulsion does not require fuel to be carried on board the spacecraft, it could enable ultra-fast, even relativistic space-flight speeds necessary for scalable space exploration[37–44].

## Results and discussion

The proof-of-concept metasurface elements for passive stabilization (MEPS) are shown in Fig. 2a, where the unit cell consists of optical resonators of subwavelength thickness on a thin substrate. We arranged the unit cells in a mirror-symmetric manner with respect to the structure's centre of mass, to eliminate the moment and lateral force when the structure is in a symmetric equilibrium position (that is, centred on the beam). An important feature of an MEPS is the asymmetry of the unit cell; as we will show below, this asymmetry ensures that a restoring torque can be generated for a structure that is rotated out of its equilibrium position. To evaluate the light-induced force on the unit cell of a particular structure and dimensions, we collected the intensity of light that is scattered into the relevant orders. For a structure of period $d$, the incident light of wavelength $\lambda$ will refract according to $m\lambda/d = \sin(\beta_m) - \sin(\theta)$, where $\theta, \beta_m$ are the incident angle and the refracted angle of order $m$, respectively. Collecting all refracted light, the total pressure ($p$) that the light exerts on the building-block unit cell can be expressed as (see Supplementary Information)

$$\mathbf{p} = -\frac{I}{c}\sum_m [t_m \sin(\beta_m - \theta) + r_m \sin(\beta_m + \theta)]\,\mathbf{e_x} + [-t_m \cos(\beta_m - \theta) + r_m \cos(\beta_m + \theta)]\,\mathbf{e_z} - \frac{I}{c}\mathbf{e_z} \quad (1)$$

where $r_m, t_m$ correspond to the (angle-dependent) reflection and transmission coefficients of the relevant orders (see Supplementary Fig. 3), respectively; $I$ is the (local) beam intensity, $c$ is the speed of light, and $\mathbf{e_x}$ and $\mathbf{e_z}$ are the unit vectors along the $x$ and the $z$ axis, respectively. Using these expressions, we can evaluate the total force ($F$) and moment ($\tau$) on a composite, mirror-symmetric structure under rotation and displacement of its centre of mass away from the axis of the Gaussian-shaped laser beam of peak intensity $I_0$ and width $w$. For compactness, these expressions are given in the Supplementary Information. We assume that the overall structure has diameter $D$ and that both the structure and the beam width are much larger than the dimensions of the unit cell, that is, $D, w \gg d$. Given the total force and torque applied by an incident beam, the rigid-body dynamics can be expressed as a first-order vector differential equation $\mathrm{d}\mathbf{u}/\mathrm{d}t = \mathrm{f}(\mathrm{u})$, where $\mathbf{u} = (z, v_z, x, v_x, \theta, \omega)^T$ is the state vector of the system, and $\mathbf{f}(\mathbf{u}) = (v_z, f_z, v_x, f_x, \omega, f_\theta)^T$, with the relevant expressions listed in the Supplementary Information. Here, we focus on the dynamics in the transverse direction, that is, orthogonal to the laser beam. Once self-restoring behaviour is achieved, the intensity of light, as well as the size and the weight of the structure, can be chosen to achieve the desired dynamics (for example, levitation, propulsion) along the beam axis.

To design the MEPS, we varied the geometric parameters $(d, x_{1,2}, w_{1,2})$ of the unit cell shown in Fig. 2a, seeking to find designs

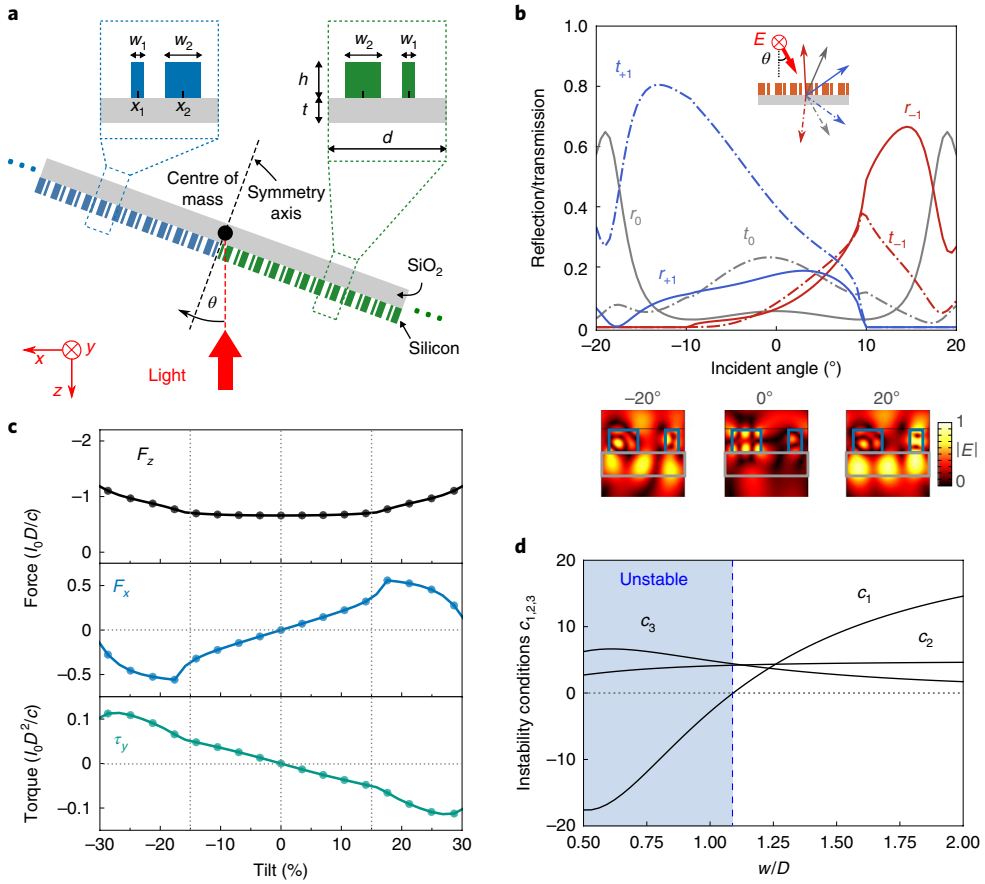


**Fig. 2 | MEPS. a**, Schematic showing symmetry with respect to the centre of mass. Insets show the elementary asymmetric unit cell of period $d$ (and its mirror image) consisting of two dissimilar rectangular resonators (widths $w_1$ and $w_2$). **b**, Reflection (solid) and transmission (dot-dashed) coefficients for various diffracting orders as a function of incident angle. Light is transverse-electric polarized (inside inset shows the direction of the electric field $E$). Inset below: normalized electric field ($|E|$) shows anisotropic optical reponse of the asymmetric unit cell at different incident angles. **c**, Light-induced force ($F_z$, $F_x$) and torque ($\tau_y$) as a function of percentage tilt/pitch $\tan\theta$. Force (torque) is per unit length in the $y$ direction in units of $I_0D/c$ ($I_0D^2/c$), where $D \gg d$. The shape of $\tau_y$—specifically, $\tau_y(\theta)\tan\theta < 0$—points to a self-restoring response. **d**, Instability conditions for dynamics near the origin ($c_{1,2,3}$). For this particular design, when $w$ is smaller than $w/D \approx 1.1$, the dynamics is guaranteed to be unstable.

that could exhibit self-stabilization (see Methods). We focus on a silicon-on-insulator platform with silicon resonators on a silica substrate that could be integrated into lightweight structures exhibiting both a high refractive index and ultra-low losses in the infrared. These features, for example, could be particularly relevant for effective space propulsion/manipulation applications, where light weight and mitigation of beam-induced heating are critical. Given this, one potential MEPS design can be realized with an asymmetric unit cell with $d = 1.8\,\mu\text{m}$, where $x_1\,(x_2) = 0.15\,(0.75)\,d$ and $w_1\,(w_2) = 0.15\,(0.35)\,d$. Here, we assume an incident beam of $\lambda = 1.5\,\mu\text{m}$, with out-of-plane (transverse-electric) polarization. The thickness of the $SiO_2$ substrate ($t$) and the height of the subwavelength silicon resonators ($h$) are chosen to be $0.5\,\mu\text{m}$. For this structure, we calculated the reflection and transmission coefficients of various diffracted orders as a function of the incident angle (Fig. 2b). By design, we observe a strong asymmetry of refraction at normal incidence, as evidenced by the dissimilar magnitudes for the $r_{\pm1}$ and $t_{\pm1}$ amplitudes. This behaviour persists for larger incident angles, stemming from the asymmetric coupling of subwavelength silicon structures to light with a positive ($\theta > 0$) or negative ($\theta < 0$) lateral wave-vector component. This anisotropic optical response is visualized in the bottom inset of Fig. 2b, which shows the magnitude of the electric field for different incident angles. When this unit cell design is integrated into the MEPS structure illustrated in Fig. 2a, we can infer the total force and torque under light illumination. Figure 2c shows the parallel and transverse forces, as well as the torque, as a function of the tilt/pitch, $\tan(\theta)$. The shown quantities are per unit length in the $y$ direction and normalized to units of $I_0D/c$ ($I_0D^2/c$ for torque). We observe that the shape of the torque curve—specifically, the functional form with $\tau_y(\theta)\tan\theta < 0$—points to a self-restoring orientation response.

To characterize the dynamics of a structure under Gaussian beam illumination, we numerically evolved in time the equations of motion. Figure 3 shows the dynamics for several initial conditions in the propulsion domain, where the radiation pressure dominates over the weight. In Fig. 3a, we assume that the structure is initially displaced from the beam axis at time $t = 0$. For this case, the centre-of-mass trajectory (Fig. 3a, middle panel) shows a confined behaviour in the lateral direction, while the structure is accelerating parallel to the beam axis. The temporal evolution of the lateral displacement and the tilt is shown in the bottom panel of Fig. 3a, where the time (abscissa) is normalized in units of $t_0 = \sqrt{m_1 c/I_0}$, with $m_1$ the mass per unit length ($y$ direction) of the structure (see Supplementary Information). As a second example, we analysed the case when a structure is initially both displaced ($-0.5D$) and tilted (10%). This is shown in Fig. 3b, and Supplementary Video 1 shows time evolution of the dynamics for this case. We further performed the sweep over a range of both initial displacements ($-0.5D$

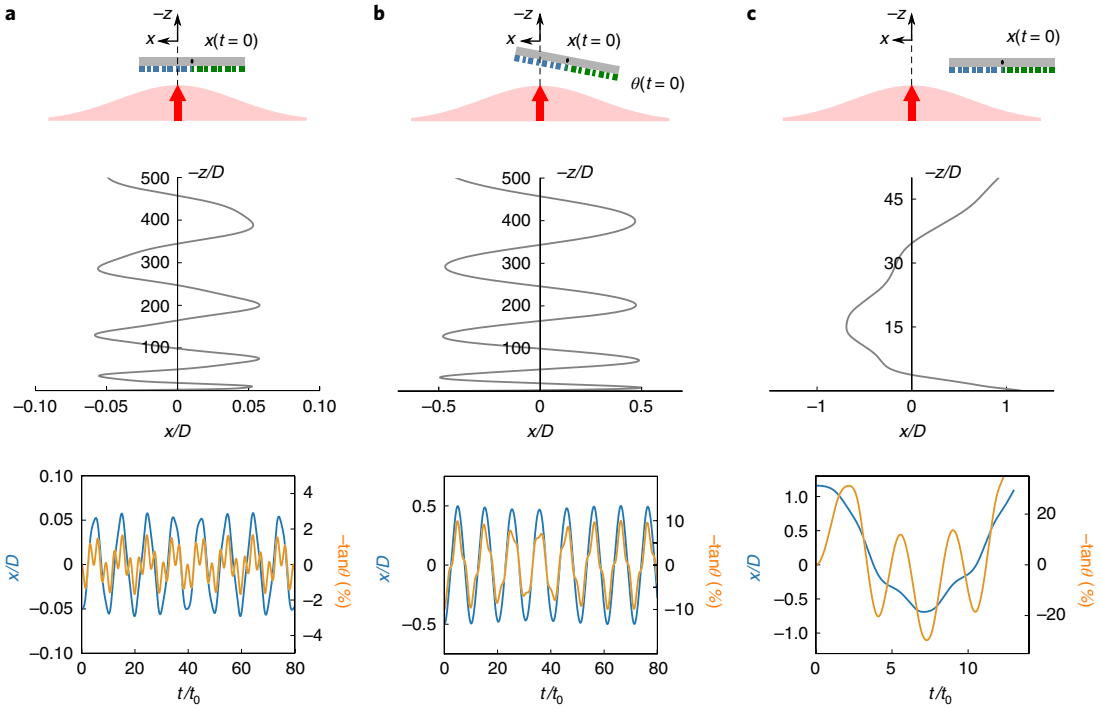


**Fig. 3 | Example dynamics of a propelled nanostructured object. a–c**, Middle row shows the trajectory of the centre of mass as a function of time, under Gaussian beam illumination, for different initial parameters (top row). Bottom row shows time evolution of the lateral displacement and tilt/pitch. The dynamics is bounded for the example cases of initial ($t=0$) lateral offset from the beam centre of $-0.05D$ with no tilt (**a**) and the initial offset of $-0.5D$ with tilt of 10% (**b**). In both cases, the observed amplitudes of dynamics remain bounded within the analysed timescale. An example of unstable dynamics is for an offset of $1.16D$ (**c**), where the structure escapes the beam. Here, $w=2D$. In the top row, the shaded red region and the arrow indicate the incident light beam.

to $0.5D$) and tilts (−10% to 10%) and observe similar bounded dynamics over the analysed timescales ($10^3 t_0$). This sweep analysis was repeated, with a small amount of white noise (~1% deviation) added to the light intensity to mimic potential variations in laser power. Again, the observed simulated dynamics remains bounded (Supplementary Information). One example of instability is shown in Fig. 3c, where the structure starts notably displaced from the origin. Although the light-induced force and torque initially direct the structure towards the beam's optical axis, it builds up too much velocity to remain confined and is subsequently driven away from the beam.

The ability of the structure to stay in the neighbourhood of the beam axis is influenced by its size relative to the width of the illuminating beam. For the example MEPS design under consideration, we can estimate this dependence by examining the elements of the Jacobian matrix (see Methods). The requirement that no eigenvalue has a positive real part can be recast as a set of three conditions $c_{1,2,3}>0$, each a function of the ratio of beam width to diameter of the structure ($w/D$). These expressions, given in Supplementary Fig. 8, are plotted in Fig. 2d. In particular, for this MEPS design, we observe that the condition $c_1=(f_{xx}-f_{\theta\theta})^2+4f_{\theta x}f_{x\theta}>0$ is violated when the beam width is smaller than $w/D\approx 1.1$, guaranteeing unstable dynamics. We note that this analytical condition is applicable near the origin and that the plotted trends of $c_i$ are specific to this particular MEPS design. For larger displacements, we resort to numerical evaluation of the equations of motion: as one example, in Supplementary Fig. 6, we show a map of the beam width and the initial displacement ($x_0$) needed to ensure that the tilt of the structure will not exceed a predetermined tilt threshold over the analysed timescale. In the Supplementary Information, we show how damping can assist with asymptotic stability of motion in the neighbourhood of the beam axis and discuss the relationship between the damping coefficients for translation and for rotation.

We note that a single MEPS can generate self-stabilizing dynamics for translations and rotations in one plane. Having established the relevant design considerations, we describe one example pathway for how multiple MEPS could be integrated in a macroscopic object to yield self-stabilization with respect to different degrees of freedom. Among the many possible ways to combine multiple MEPS, here we focus on a square-like structure, depicted in Fig. 4a and shown in detail in Supplementary Fig. 8. As before, this structure maintains symmetry with respect to its centre of mass and consists of opposing elements that provide the restoring pitch ($\theta$), roll ($\phi$) and yaw ($\psi$) torque. For this configuration, we show that combining two different MEPS could in principle be sufficient (schematically shown in Fig. 4b). Nanophotonic design of these elements is dictated by the orientation of the structure relative to the polarization of the impinging light. For example, to achieve roll-restoring behaviour, we designed an MEPS in region B to operate for predominantly transverse-magnetic polarization. Similarly, for pitch-restoring behaviour, the predominant polarization for region A will be transverse-electric polarization. Here, we reused the same design from Fig. 2. For region B, we also rotated the elements by an angle $\delta$ relative to the $y$ axis of the structure. The purpose of this rotation was to introduce the $\psi$-dependence of the torque that is self-restoring, leading to yaw torque in the macroscopic structure. As such, the macroscopic structure could exhibit polarization-locking, where its orientation is pinned to the polarization direction of the incident light. Correspondingly, the structure could be oriented around the beam axis by rotating the polarization of the light beam.

Figure 4c shows light-induced forces and torques as a function of the corresponding tilt, given in normalized units of $I_0D^2/c$ and $I_0D^3/c$, respectively. We observe restoring components of the torque, namely, $\tau_i(\beta)\tan\beta<0$ (for $i=x,y,z$ and $\beta=\phi,\theta,\psi$, respectively). We note that $\tau_z$ is noticeably smaller than $\tau_{x,y}$ (in part because the chosen angle of rotation $\delta=10^o$ is small), which limits robustness

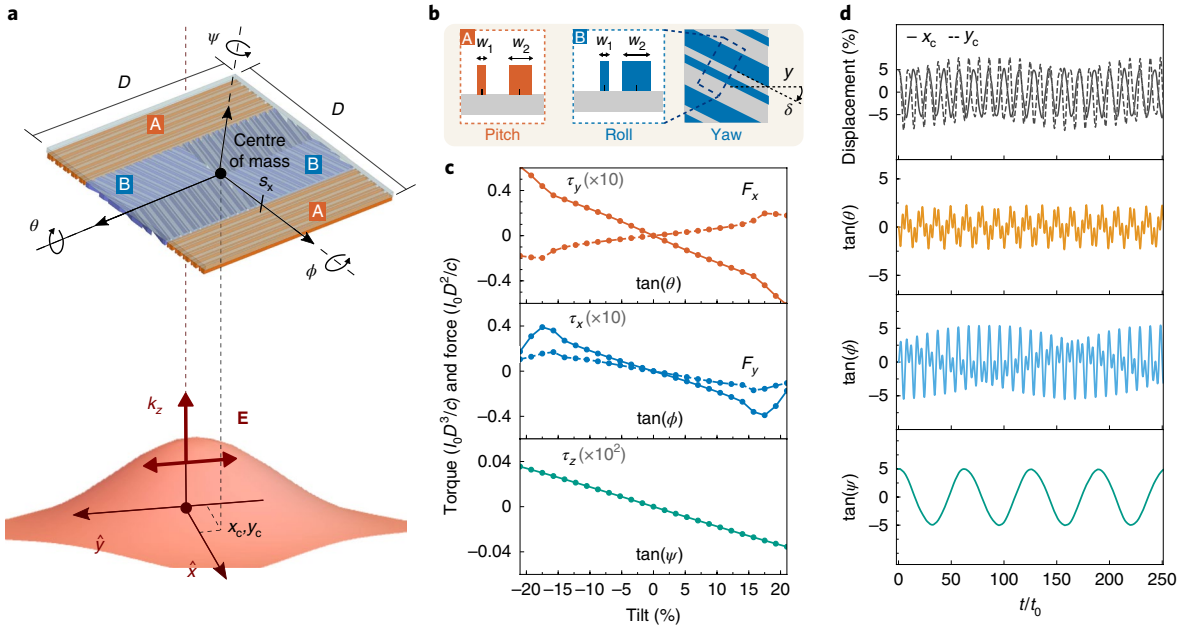


**Fig. 4 | Towards composite passively self-stabilizing structures. a**, One example, consisting of multiple MEPS that could provide the pitch-, roll- and yaw-restoring behaviour. The polarization (**E**) and the direction ($k_z$) of the incident field, as well as the centre-of-mass displacement ($x_c$,$y_c$) is shown relative to the *x* and the *y* axes. **b**, Schematic of the two building-block elements, one rotated by an angle relative to the *y* axis, to provide restoring yaw torque. The object consists of a silica substrate base with silicon resonators. **c**, Corresponding values for the force–torque pairs, as a function of the percentage tilt. The beam is polarized along the *y* axis. **d**, Time evolution of equations of motion shows an example of restoring behaviour for rotation and translation.

against yaw displacement. Finally, we evolved the coupled equations of motion to show an example response (Fig. 4d) for initial displacement (5% along *x*,*y*) and yaw tilt (5%). Here, the corresponding units of time are normalized in units of $t_0 = \sqrt{mc/I_0D}$. As one example of probing some neighbourhood around the equilibrium, we sampled possible combinations of displacement $x, y = \pm 5\%$ and tilt $\phi, \theta, \psi = \pm 5\%$ and observe bounded dynamics over the analysed timescale ($10^3 t_0$). However, we emphasize that this analysis sampled a very small portion of the available phase space and does not imply bounded behaviour for parameters or timescales other than those considered. The exploration of the ten-dimensional phase space of such a rigid body in a light field, as well as identification of the basin of attraction, warrant further study in these and other photonic motifs shown in Fig. 1. Nevertheless, these observations point to such integration of MEPS structures as a potential pathway towards stability.

**Summary and outlook.** We have shown that structuring the object's surface on the nanoscale could impart self-restoring behaviour for optical manipulation. Among our main results, we find that engineered anisotropy of scattering is required, that a centrally symmetric arrangement relative to the centre of mass is beneficial, and that a class of subwavelength elements, consisting of dielectric resonators with an asymmetric unit cell, can impart mechanical stabilization when the structure is tilted and/or displaced from the beam axis. With such self-restoring behaviour, the light intensity, size and weight of the structure can be chosen to achieve the desired dynamics (levitation, propulsion) along the axial (*z*) direction. Because mechanical stabilization arises from optical anisotropy on the object's surface and not from focusing the beam, stabilization should be achievable over long interaction distances using collimated beams.

For proof-of-concept purposes, here we have focused on macroscopically flat objects, where the mass distribution is uniform and the expressions for moments of inertia are correspondingly simple. Nevertheless, as highlighted by our derivations (see Supplementary Information), the proposed approach of tailoring the refraction of light along the surface via engineered nanostructures could also apply to non-planar objects and to objects with non-uniform mass distributions. Although we assume ideal conditions, in practice, there will be damping in the system, either from the environment or through engineered coupling to mechanical modes of the structure, which can assist with asymptotic stability (see the discussion in Supplementary Information). Similarly, active feedback schemes can be incorporated. As a demonstration that this photonic manipulation approach does not require high absorption or high reflectance, we chose materials with very low loss. Other materials, including metals or semiconductors in the absorbing spectral range, could be included, depending on the application. We stress that the results presented here are not optimized and are intended to showcase the potential of the proposed approach for controlled mechanical manipulation.

We envision a number of compelling extensions of this work. As one example, the proposed scheme could be used to realize a levitated macroscopic mechanical oscillator, as a unique platform for probing quantum and classical optomechanics[45] and phase-space dynamics[46]. Here, we focused on the wavelength regime where absorption in silicon and silica is minimized. For applications where heating effects need to be mitigated, radiative cooling properties of silica can be used[47]. Conversely, a self-stabilizing structure could also be used in conjunction with photophoretic effects such as thermal gradients generated by optically induced heating. Manipulation techniques based on photophoresis[48–52] rely on absorption and environmental mediators (for example, gas particles), but could be combined with the proposed approach in gaseous environments for a greater degree of dynamic control. Although our work is focused on engineering the optical response along the object's surface, it would be intriguing to combine it with a metalens design for structuring the light beam[53,54], potentially enabling novel ways of optical 'pulling'[55,56]. Moving away from the rigid-body framework, as well as consideration of large displacements or spinning configurations, are also relevant directions for future research.

One potential application of this work is for directed energy propulsion in space. The prospects for concepts such as solar- and laser-propelled light sails could be advanced by using self-stabilizing dynamics, in addition to recent ideas behind diffractive optics for sailcraft radiation pressure control[42,57]. Among applications in space, it is perhaps most intriguing to consider light sails accelerated by high-power lasers, potentially to ultra-fast velocities[40]. To account for the Doppler shift in such a system, we envision leveraging the design principles behind broadband metasurfaces[30]. Ultra-light, ultra-low-loss[47] versions of the passively stabilized laser-propelled structures could be essential for realizing such audacious applications.

## Online content

Any methods, additional references, Nature Research reporting summaries, source data, statements of data availability and associated accession codes are available at https://doi.org/10.1038/s41566-019-0373-y.

Received: 17 September 2018; Accepted: 29 January 2019;
Published online: 18 March 2019

## References

1. Ashkin, A. Acceleration and trapping of particles by radiation pressure. *Phys. Rev. Lett.* **24**, 156–159 (1970).
2. Ashkin, A., Dziedzic, J. M., Bjorkholm, J. E. & Chu, S. Observation of a single-beam gradient force optical trap for dielectric particles. *Opt. Lett.* **11**, 288–290 (1986).
3. Grier, D. G. A revolution in optical manipulation. *Nature* **424**, 810–816 (2003).
4. Baumgartl, J., Mazilu, M. & Dholakia, K. Optically mediated particle clearing using Airy wavepackets. *Nat. Photon.* **2**, 675–678 (2008).
5. Padgett, M. & Bowman, R. Tweezers with a twist. *Nat. Photon.* **5**, 343–348 (2011).
6. Woerdemann, M., Alpmann, C., Esseling, M. & Denz, C. Advanced optical trapping by complex beam shaping. *Laser Photon. Rev.* **7**, 839–854 (2013).
7. Taylor, M. A., Waleed, M., Stilgoe, A. B., Rubinsztein-Dunlop, H. & Bowen, W. P. Enhanced optical trapping via structured scattering. *Nat. Photon.* **9**, 669–673 (2015).
8. Stevenson, D. J., Gunn-Moore, F. & Dholakia, K. Light forces the pace: optical manipulation for biophotonics. *J. Biomed. Opt.* **15**, 41503 (2010).
9. Fazal, F. M. & Block, S. M. Optical tweezers study life under tension. *Nat. Photon.* **5**, 318–321 (2011).
10. MacDonald, M. P., Spalding, G. C. & Dholakia, K. Microfluidic sorting in an optical lattice. *Nature* **426**, 421–424 (2003).
11. Padgett, M. & Di Leonardo, R. Holographic optical tweezers and their relevance to lab on chip devices. *Lab Chip* **11**, 1196–1205 (2011).
12. Grier, D. G. Optical tweezers in colloid and interface science. *Curr. Opin. Colloid In.* **2**, 264–270 (1997).
13. Chang, D. E. et al. Cavity opto-mechanics using an optically levitated nanosphere. *Proc. Natl Acad. Sci. USA* **107**, 1005–1010 (2009).
14. Romero-Isart, O., Juan, M. L., Quidant, R. & Cirac, J. I. Toward quantum superposition of living organisms. *New J. Phys.* **12**, 33015 (2010).
15. Li, T., Kheifets, S. & Raizen, M. G. Millikelvin cooling of an optically trapped microsphere in vacuum. *Nat. Phys.* **7**, 527–530 (2011).
16. Gieseler, J., Deutsch, B., Quidant, R. & Novotny, L. Subkelvin parametric feedback cooling of a laser-trapped nanoparticle. *Phys. Rev. Lett.* **109**, 103603 (2012).
17. Neukirch, L. P., von Haartman, E., Rosenholm, J. M. & Nick Vamivakas, A. Multi-dimensional single-spin nano-optomechanics with a levitated nanodiamond. *Nat. Photon.* **9**, 653–657 (2015).
18. Ricci, F. et al. Optically levitated nanoparticle as a model system for stochastic bistable dynamics. *Nat. Commun.* **8**, 15141 (2017).
19. Bhattacharya, M., Vamivakas, A. N. & Barker, P. Levitated optomechanics: introduction. *J. Opt. Soc. Am. B* **34**, LO1–LO2 (2017).
20. Cihan, A. F., Curto, A. G., Raza, S., Kik, P. G. & Brongersma, M. L. Silicon Mie resonators for highly directional light emission from monolayer $MoS_2$. *Nat. Photon.* **12**, 284–290 (2018).
21. Kuznetsov, A. I., Miroshnichenko, A. E., Brongersma, M. L., Kivshar, Y. S. & Luk'yanchuk, B. Optically resonant dielectric nanostructures. *Science* **354**, aag2472 (2016).
22. Joannopoulos, J. D., Johnson, S. G., Winn, J. N. & Meade, R. D. *Photonic Crystals: Molding the Flow of Light* 2nd edn (Princeton Univ. Press, 2008).
23. Fattal, D., Li, J., Peng, Z., Fiorentino, M. & Beausoleil, R. G. Flat dielectric grating reflectors with focusing abilities. *Nat. Photon.* **4**, 466–470 (2010).
24. Kamali, S. M., Arbabi, E., Arbabi, A. & Faraon, A. A review of dielectric optical metasurfaces for wavefront control. *Nanophotonics* **7**, 1041–1068 (2018).
25. Yu, N. et al. Light propagation with phase discontinuities: generalized laws of reflection and refraction. *Science* **334**, 333–337 (2011).
26. Aieta, F. et al. Out-of-plane reflection and refraction of light by anisotropic optical antenna metasurfaces with phase discontinuities. *Nano Lett.* **12**, 1702–1706 (2012).
27. Kildishev, A. V., Boltasseva, A. & Shalaev, V. M. Planar photonics with metasurfaces. *Science* **339**, 1232009 (2013).
28. Monticone, F., Estakhri, N. M. & Alù, A. Full control of nanoscale optical transmission with a composite metascreen. *Phys. Rev. Lett.* **110**, 203903 (2013).
29. Lin, D., Fan, P., Hasman, E. & Brongersma, M. L. Dielectric gradient metasurface optical elements. *Science* **345**, 298–302 (2014).
30. Yu, N. & Capasso, F. Flat optics with designer metasurfaces. *Nat. Mater.* **13**, 139–150 (2014).
31. Arbabi, A., Arbabi, E., Horie, Y., Kamali, S. M. & Faraon, A. Planar metasurface retroreflector. *Nat. Photon.* **11**, 415–420 (2017).
32. Genevet, P., Capasso, F., Aieta, F., Khorasaninejad, M. & Devlin, R. Recent advances in planar optics: from plasmonic to dielectric metasurfaces. *Optica* **4**, 139–152 (2017).
33. Swartzlander, G. A., Peterson, T. J., Artusio-Glimpse, A. B. & Raisanen, A. D. Stable optical lift. *Nat. Photon.* **5**, 48–51 (2010).
34. Srinivasan, P. et al. Stability of laser-propelled wafer satellites. In *Planetary Defense and Space Environment Applications* (ed. Hughes, G. B.) 998105 (Conference Series Vol. 9981, SPIE, 2016).
35. Manchester, Z. & Loeb, A. Stability of a light sail riding on a laser beam. *Astrophys. J. Lett.* **837**, L20 (2017).
36. Popova, H., Efendiev, M. & Gabitov, I. On the stability of a space vehicle riding on an intense laser beam. Preprint at https://arxiv.org/abs/1610.08043 (2016).
37. Marx, G. Interstellar vehicle propelled by terrestrial laser beam. *Nature* **211**, 22–23 (1966).
38. Redding, J. L. Interstellar vehicle propelled by terrestrial laser beam. *Nature* **213**, 588–589 (1967).
39. Forward, R. L. Roundtrip interstellar travel using laser-pushed lightsails. *J. Spacecraft Rockets* **21**, 187–195 (1984).
40. Breakthrough Starshot *Breakthrough Initiatives* https://breakthroughinitiatives.org/Initiative/ (2018).
41. Lubin, P. A roadmap to interstellar flight. *J. Br. Interplanet. Soc.* **69**, 40–72 (2016).
42. Swartzlander, G. A. Radiation pressure on a diffractive sailcraft. *J. Opt. Soc. Am. B* **34**, C25–C30 (2017).
43. Atwater, H. A. et al. Materials challenges for the Starshot lightsail. *Nat. Mater.* **17**, 861–867 (2018).
44. Kulkarni, N., Lubin, P. & Zhang, Q. Relativistic spacecraft propelled by directed energy. *Astron. J.* **155**, 155 (2018).
45. Guccione, G. et al. Scattering-free optical levitation of a cavity mirror. *Phys. Rev. Lett.* **111**, 183001 (2013).
46. Ilic, O. et al. Topologically enabled optical nanomotors. *Sci. Adv.* **3**, e1602738 (2017).
47. Ilic, O., Went, C. M. & Atwater, H. A. Nanophotonic heterostructures for efficient propulsion and radiative cooling of relativistic light sails. *Nano Lett.* **18**, 5583–5589 (2018).
48. Jiang, H.-R., Yoshinaga, N. & Sano, M. Active motion of a Janus particle by self-thermophoresis in a defocused laser beam. *Phys. Rev. Lett.* **105**, 268302 (2010).
49. Qian, B., Montiel, D., Bregulla, A., Cichos, F. & Yang, H. Harnessing thermal fluctuations for purposeful activities: the manipulation of single micro-swimmers by adaptive photon nudging. *Chem. Sci.* **4**, 1420–1429 (2013).
50. Shvedov, V., Davoyan, A. R., Hnatovsky, C., Engheta, N. & Krolikowski, W. A long-range polarization-controlled optical tractor beam. *Nat. Photon.* **8**, 846–850 (2014).
51. Ilic, O., Kaminer, I., Lahini, Y., Buljan, H. & Soljačić, M. Exploiting optical asymmetry for controlled guiding of particles with light. *ACS Photon.* **3**, 197–202 (2016).
52. Lu, J. et al. Light-induced pulling and pushing by the synergic effect of optical force and photophoretic force. *Phys. Rev. Lett.* **118**, 043601 (2017).
53. Tkachenko, G. et al. Optical trapping with planar silicon metalenses. *Opt. Lett.* **43**, 3224–3227 (2018).
54. Markovich, H., Shishkin, I. I., Hendler, N. & Ginzburg, P. Optical manipulation along an optical axis with a polarization sensitive meta-lens. *Nano Lett.* **18**, 5024–5029 (2018).
55. Dogariu, A., Sukhov, S. & Sáenz, J. Optically induced 'negative forces'. *Nat. Photon.* **7**, 24–27 (2012).
56. Chen, J., Ng, J., Lin, Z. & Chan, C. T. Optical pulling force. *Nat. Photon.* **5**, 531–534 (2011).
57. Achouri, K. & Caloz, C. Metasurface solar sail for flexible radiation pressure control. Preprint at https://arxiv.org/abs/1710.02837 (2017).

## Acknowledgements
The authors thank colleagues from the Breakthrough Starshot Lightsail committee for discussions, and acknowledge financial support from the Air Force Office of Scientific Research under grant number FA9550-16-1-0019. The authors also acknowledge discussions with A. Davoyan, O. Miller, Z. Manchester, M. Kelzenberg, I. Kaminer, C. Went, W. Whitney, M. Sherrott, J. Wong, D. Jariwala, P. Jha and H. Akbari.

## Author contributions
All authors discussed the results and made critical contributions to the work.

## Competing interests
The authors declare no competing interests.

## Additional information
**Supplementary information** is available for this paper at https://doi.org/10.1038/s41566-019-0373-y.

**Reprints and permissions information** is available at www.nature.com/reprints.

**Correspondence and requests for materials** should be addressed to H.A.A.

**Publisher's note:** Springer Nature remains neutral with regard to jurisdictional claims in published maps and institutional affiliations.

## Methods

All numerical electromagnetic simulations were performed using the finite-element-method solver COMSOL Multiphysics (http://www.comsol.com). For materials analysed in this work, we assume indices of refraction of $n=3.5$ for silicon and $n=1.45$ for silica at the applicable wavelength of interest. Periodic boundary conditions were applied to the unit cell boundaries, and the incident electromagnetic field was linearly polarized. To find candidate MEPS designs, we varied the unit cell parameters: the unit cell size and the positions, widths and height of the silicon resonators. For simplicity, we restricted the search space to structures that support only $m=\pm 1$ non-zero orders. The presence of positive eigenvalues in the Jacobian matrix for system dynamics indicates instability. Here, we sought designs that avoid guaranteed instability, as a means of identifying candidate structures whose restoring behaviour is probed, over a certain timescale, by numerically evolving the equations of motion (see Supplementary Information).

For a given design, the direction of the incident field was varied accordingly, and the forces and torques were evaluated and stored. The unit cell pressure can either be evaluated by collecting the relevant orders (equation ( 1)) or by integrating the Maxwell stress tensor around the unit cell. In the Supplementary Information, we compare the two approaches and find excellent agreement. For Fig. 2, the incident field variation is the rotation along a single axis; for Fig. 4, the variation is simultaneously over all three Euler angles. Force/torque values were subsequently used (with linear interpolation in Fig. 3 and grid interpolation in Fig. 4) in numerical simulations where the coupled equations of motion are evolved in time. In all cases, the impinging laser is assumed to be linearly polarized along the $y$ axis. The boundaries of MEPS elements in the larger structure are described by the parameter $s_x$, where $0<s_x<\frac{1}{2}$. In the example shown in Fig. 4, regions A and B occupy the same area ($s_x=1/4$), with $d^B=1.775\,\mu\text{m}$, $x_1^B(x_2^B)=0.15(0.75)d^B$, $w_1^B(w_2^B)=0.125(0.25)d^B$, $\delta=10°$, $h^B=0.45\,\mu\text{m}$ and $w=2D$. There is a uniform substrate layer ($t=0.5\,\mu\text{m}$) of silica. Because of the nature of the coupled equations of motion in the absence of damping, linearization can be used to indicate instability, but not to draw conclusions about stability. As such, the observed restoring behaviour may not apply for parameters or timescales other than those considered here. Although the considered timescales are finite, we observe that the structure can traverse $>10^6D$ distance in the direction of the beam while staying in the vicinity of the beam axis. Introducing damping (as discussed in the Supplementary Information) is a way to facilitate asymptotic stability for motion near the beam axis.

## Data availability

The data that support the plots within this paper and other findings of this study are available from the corresponding author upon reasonable request.